Int. J. Solids Structures, Vol. 17, No. 12, pp. 1135–1147, 1981
Printed in Great Britain.

0020-7683/81/121135-13$02.00/0

EFFECTIVE WIDTHS OF RECTANGULAR SLABS STIFFENED ALONG TWO OPPOSITE EDGES BY PRESTRESSED EDGE BEAMS

A. O. ADEKOLA
Office of the Vice-Chancellor, Federal University of Technology, Bauchi, Nigeria

Received 2 *June* 1980; *in revised form* 19 *January* 1981)

Abstract—The present analysis is an attempt to determine the portion of a rectangular slab that is acting with its two parallel stiffening edge beams, through which prestressing loads are applied to the entire section, in resisting load. Employing the well known theories of bending of plates and beams, the constitutive equations governing the behaviour of this type of composite system are presented. In particular, the equation of compatibility of strains between the slab edges and the stiffening edge beams at their junctions is formulated. In doing this, the biaxial nature of the bending of the edge beams, ignored in earlier formulations[1], has been incorporated. The results of the present analysis show that, under transverse loading, the portion of the slab, called the *effectiv width*, that can be considered effective as a part of each of the stiffening edge beams in determining stresses and deflexions is not significantly different from that obtained for an unprestressed section or a simply reinforced section. The effective width of the slab when such a section is subjected to only prestressing loads however shows a significant difference. We conclude from this that a single table of effective widths could be adopted for design purposes when considering transverse bending of this type of composite system whether the section is prestressed or not. Typical stress distributions due to (i) prestress alone, (ii) transverse loading alone and (ii) combined prestress and transverse loading are presented to demonstrate that the present formulation is versatile enough to solve problems involving prestressed edge beams in this type of composite assembly.

INTRODUCTION

The analysis of a rectangular slab of constant thickness, simply supported at two opposite edges and having identical edge beams integral with the slab along the other two edges was first presented by Allen and Severn[1]. Their presentation was aimed at verifying the reliability of theoretical stresses and deflexions obtained from their assumed mathematical model with experimental results. They succeeded in that regard. In the present analysis we are concerned with the determination of suitable mathematical model that will enable us determine effective widths of the slab acting with each of the two edge beams when the edge beams may themselves be subject to prestressing load in addition to transverse loading. One significant difference between the present formulation and that due to Allen and Severn is the incorporation in the present analysis of biaxial bending of the edge ribs in the determination of longitudinal bending strains at the edge beams when formulating the strain compatibility condition between slab and beam. This means that our eqns (24) and (25) represent a more correct and complete model of joint strain compatibility condition than the corresponding one due to Allen and Severn.

NOTATION

a	span
A	edge beam cross-sectional area
b	half width of slab
b_r	width of edge beam at junction with slab
C	torsional couple in edge beam
D	cylindrical stiffness of slab
e_m	maximum eccentricity of prestressing force
E	elastic modulus of concrete
EI	flexural rigidity of edge beam about major axis
Ei	flexural rigidity of edge beam about minor axis
F	axial force between slab and edge beam
$\bar{h}$	distance between centroidal axis of edge beam and slab
H	overall depth of edge beam
K	torsional rigidity of edge beam
M_r, M_T	bending moments in edge beam
M_{xx}, M_{yy}	direct bending moment in slab
M_{xy}	torsional bending moment in slab

n, m number of harmonics
p intensity of uniformly distributed loading
P prestressing force
q superimposed slab loading
t slab thickness
u_x, u_y extensional deformations in slab
V_{yb} Kirchoff's shear at slab–beam junction edge of slab
V_{xx}, V_{yy} Kirchoff's shears at plate edges
w transverse deflexion
W transverse point load
x, y Cartesian coordinates
$\sigma_{xx}, \sigma_{yy}, \sigma_{xy}$ membrane stresses in slab
μ Poisson's ratio
ϕ stress function

GOVERNING EQUATIONS

Bending

The deflexion field, w, for an elastic isotropic plate subjected to transverse loading is governed by

$$\nabla^4 w = \frac{q}{D} \tag{1}$$

where ∇^4 denotes the two dimensional biharmonic operator and D the cylindrical stiffness of the slab.

Using the system of coordinates (x, y) shown in Fig. 1 and assuming a symmetric loading with respect to the y coordinate, a suitable series solution of eqn (1) in respect of a rectangular slab simply supported at $x = 0$ and $x = a$ is given by

$$w = \left[\frac{\lambda_n^{-4} q}{D} + A_{n1} ch\lambda_n y + D_{n1}\lambda_n y sh\lambda_n y\right] \sin \lambda_n x \tag{2}$$

where $\lambda_n = (2n - 1)(\pi/a)$, and for convenience we omit the summation sign of the series over n.

Noting that the expressions for bending moment, M_{yb}, and Kirchoff's shears V_{yb} at the edges $y = \pm b$ of a plate are derivable from the expressions

$$\left.\begin{aligned} M_{yy} &= -D[w_{,yy} + \mu w_{,xx}] \\ V_{yy} &= -D[w_{,yy} + (2-\mu)w_{,xx}], y \end{aligned}\right\} \tag{3}$$

we deduce that

$$M_{yyb} = (1-\mu)\lambda_n^2 D\left[\frac{4\mu q}{(1-\mu)\lambda_n^5 aD} - A_{n1} ch\psi - D_{n1}\left(\psi sh\psi + \frac{2}{1-\mu} ch\psi\right)\right] \sin \lambda_n x \tag{4}$$

$$V_{yyb} = (1-\mu)\lambda_n^3 D\left[A_{n1} sh\psi + D_{n1}\left(\psi ch\psi - \frac{1+\mu}{1-\mu} \cdot sh\psi\right)\right] \sin \lambda_n x \tag{5}$$

where $\psi = \lambda_n b$.

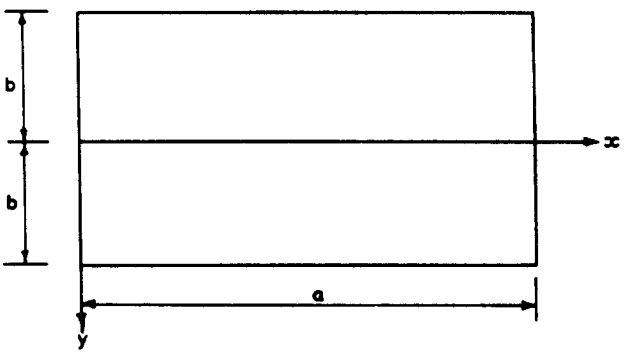

Fig. 1.

Stretching

To obtain the complete stress distribution in the plate we must adjoin to the deflexion field the displacement fields in terms of the Airys stress function, ϕ, which define the plane-stress and in-plane displacements as follows:

$$\left.\begin{aligned} \sigma_{xx} &= \phi_{,yy} \\ \sigma_{yy} &= \phi_{,xx} \\ \sigma_{xy} &= \phi_{,xy} \\ Eu_{x,x} &= \sigma_{xx} - \mu\sigma_{yy} \\ Eu_{y,y} &= \sigma_{yy} - \mu\sigma_{xx} \end{aligned}\right\} \tag{6}$$

where (u_x, u_y) denotes the displacement vector, E the elastic modulus, μ Poisson's ratio, while the function ϕ satisfies the biharmonic equation

$$\nabla^4\phi = 0. \tag{7}$$

Assuming stress free edges at $x = 0$ and $x = a$, i.e. $\sigma_{xx} = \sigma_{xy} = 0$, and also symmetrical loading with respect to the y axis, we construct a suitable series solution of eqn (7) as

$$\phi = [A_{n2}ch\lambda_n y + D_{n2}\lambda_n y sh\lambda_n y]\sin\lambda_n x - \frac{E_{n2}}{a}\cos\alpha_n y[(x-a)sh\alpha_n x + xsh\alpha_n(x-a)] \tag{8}$$

provided

$$E_{n2} = \frac{2a/b}{\alpha_n a + sh\alpha_n a}\sum_{r=1}^{\infty}\frac{\lambda_r^2}{\lambda_r^2+\alpha_n^2}\left[A_{r2}sh\psi_r + D_{r2}\left(\psi_r ch\psi_r + \frac{\alpha_n^2-\lambda_r^2}{\lambda_r^2+\alpha_n^2}\cdot sh\psi_r\right)\right] \tag{9}$$

$$\alpha_n = (2n-1)\frac{\pi}{b}$$

$$\psi_r = \lambda_r b.$$

By the application of relevant equations in (6) above, we obtain expressions for certain stresses, displacement component and longitudinal strain at the edge of the slab $y = b$ as follows:

$$\begin{aligned} \sigma_{yyb} = &-\lambda_n^2[A_{n2}ch\psi + D_{n2}\psi sh\psi]\sin\lambda_n x \\ &+\frac{\alpha_n E_{n2}}{a}[\alpha_n(x-a)sh\alpha_n x + \alpha_n x sh\alpha_n(x-a) + 2ch\alpha_n x + 2ch\alpha_n(x-a)] \end{aligned} \tag{10}$$

$$\sigma_{xyb} = -\lambda_n^2[A_{n2}sh\psi + D_{n2}(\psi sh\psi + sh\psi)]\cos\lambda_n x \tag{11}$$

$$U_{yb} = -(1+\mu)E^{-1}\lambda_n\left[A_{n2}sh\psi + D_{n2}\left(\psi ch\psi - \frac{1-\mu}{1+\mu}\cdot sh\psi\right)\right]\sin\lambda_n x \tag{12}$$

$$\begin{aligned} e_{xxb} = &(1+\mu)E^{-1}\left\{\lambda_n^2\left[A_{n2}ch\psi + D_{n2}\left(\psi sh\psi + \frac{2}{1+\mu}\cdot ch\psi\right)\right]\sin\lambda_n x - \frac{\alpha_n E_{n2}}{a}\right. \\ &\left.\times\left[\alpha_n(x-a)sh\alpha_n x + \alpha_n x sh\alpha_n(x-a) + \frac{2\mu}{1+\mu}(ch\alpha_n x + ch\alpha_n(x-a))\right]\right\}. \end{aligned} \tag{13}$$

CONSTITUTIVE EQUATIONS ESTABLISHING INTERACTION BETWEEN SLAB AND EDGE BEAMS

For convenience, the constitutive equations needed to solve this problem completely are derived in the order in which they are employed in a subsequent computer program.

Equilibrium about the major axis

Noting that the edge rib subjected to bending moment due to the interacting axial forces F between beam and slab, as well as to bending due to transverse deflexion about its major axis, then we can express the total moment of resistance, M_T, exhibited by the rib as

$$M_T = M_r + \bar{h}F \tag{14}$$

where M_r is the moment of resistance of the rib alone in the absence of the interacting axial force F.

Considering the vertical equilibrium of the edge beam, we have

$$\delta S - (V_{yb} - p)\delta x = 0 \tag{15}$$

Hence, noting that $S_{,x} = M_{T,xx}$ eqns (14) and (15) combine to become

$$M_{r,xx} + \bar{h}F_{,xx} - V_{yb} + p = 0 \tag{16}$$

where $M_r = -EIw_{b,xx}$ and $F = -t\phi_{,y}|_{y=b}$.

Employing the expressions previously determined for w and ϕ and for the Kirchoffs shear V_{yb}, we reduce eqn (16) to

$$\begin{aligned}&[\lambda_m^4 EIch\psi_m + (1-\mu)\lambda_m^3 Dsh\psi_m]A_{m1} + [\lambda_m^4 EI\psi_m sh\psi_m \\ &+ (1-\mu)\lambda_m^3 D(\psi_m ch\psi_m - (1+\mu)(1-\mu)_x^{-1} sh\psi_m]D_{m1} \\ &- [\lambda_m^3 t\bar{h}sh'_m]A_{m2} - [\lambda_m^3 t\bar{h}(\psi_m ch\psi_m + sh\psi_m)]D_{m2} = p_m - \frac{EIq_m}{D}\end{aligned} \tag{17}$$

where $q_m = 4(\lambda_m a)_q^{-1}$,

Torsional equilibrium

Considering the forces on the edge beam as shown in Fig. 2(a), the torsional couple, C, on the beam is given by

$$C = \frac{b_r}{2} \cdot V_{yb} + M_{yb} - t\bar{h} \cdot \sigma_{yyb}. \tag{18}$$

Hence

$$-kw_{,xxy} + t\bar{h} \cdot \sigma_{yyb} - \frac{b_r}{2} \cdot V_{yb} - M_{yb} = 0. \tag{19}$$

Using the relations previously derived for σ_{yyb}, V_{yb}, M_{yb} and w in eqn (19) and multiplying the equation by $\sin \lambda_m x$ and then integrating with respect to x from 0 to a, we make use of the well known trigonometric orthogonality relations and the following definite integral

$$\int_0^a \{\alpha_r(x-a)sh\alpha_r x + \alpha_r x sh\alpha_r(x-a) + 2ch\alpha_r x + 2ch\alpha_r(x-a)\} \sin \lambda_m x \, dx = \frac{4\lambda_m(1+ch\alpha_r a)}{(\lambda_m^2 + \alpha_r^2)^2}$$

to reduce the equation to the following

$$\begin{aligned}&\left[\lambda_m K sh\psi_m - (1-\mu)\frac{\lambda_m b_r}{2} Dsh\psi_m + (1-\mu)Dch\psi_m\right]A_{m1} + \left[\lambda_m K(\psi_m ch\psi_m + sh\psi_m) - 2^{-1}\right. \\ &\times (1-\mu)\lambda_m b_r D(\psi_m ch\psi_m - (1+\mu)(1-\mu)^{-1} sh\psi_m) \\ &+ (1-\mu)D(\psi_m sh\psi_m + \cdots + 2(1-\mu)^{-1} ch\psi_m)]D_{m1} \\ &- [t\bar{h}ch\psi_m]A_{m2} - [t\bar{h}\psi_m sh\psi_m]D_{m2} + t\bar{h}\sum_{s=1}^{\infty}\sum_{r=1}^{\infty} H_{mr}[G_{rs}A_{s2} + F_{rs}D_{s2}] = 4\mu\lambda_m^{-5}a^{-1}q\end{aligned} \tag{20}$$

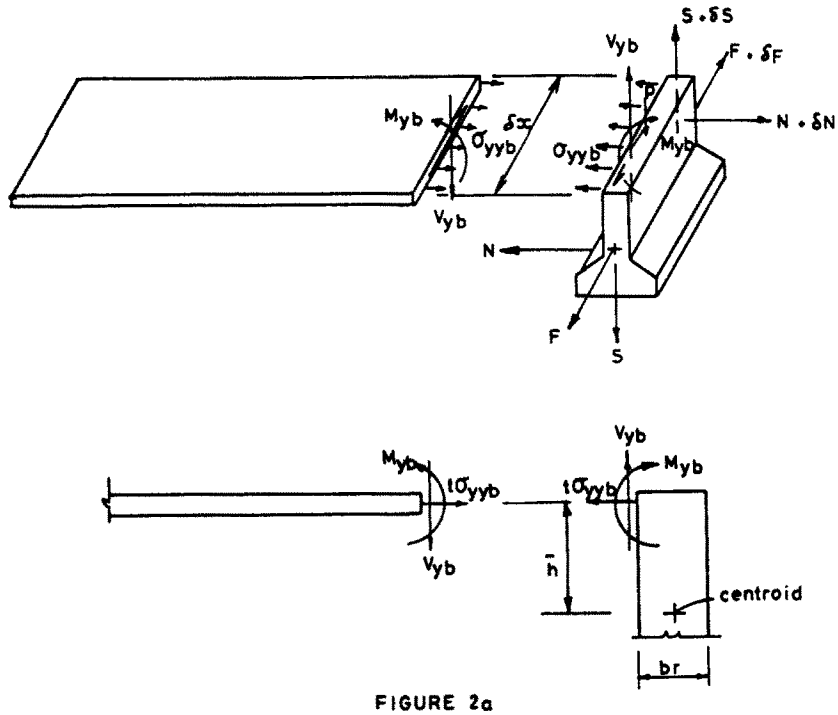

FIGURE 2a

Fig. 2.

where

$$H_{mr} = \frac{8}{a^2} \cdot \frac{\alpha_r \lambda_m (1 + ch\alpha_r a)}{(\lambda_m^2 + \alpha_r^2)^2} \tag{21}$$

$$G_{rs} = \frac{2a/b}{\alpha_r a + sh\alpha_r a} \cdot \frac{\lambda_s^2}{\lambda_s^2 + \alpha_r^2} \cdot sh\lambda_s b \tag{22}$$

$$F_{rs} = \frac{2a/b}{\alpha_r a + sh\alpha_r a} \frac{\lambda_s^2}{\lambda_r^2 + \alpha_r^2} \left[\lambda_s b ch\lambda_s b + \frac{\alpha_r^2 - \lambda_s^2}{\lambda_r^2 + \alpha_r^2} sh\lambda_s b \right]. \tag{23}$$

Junction strain compatibility condition

Two of the conditions needed in arriving at the required number of constitutive equations in order to make our present problem soluble, are obtained from the conditions of bending of the edge beam about its major and minor axes. These conditions of biaxial bending imply that the longitudinal strains in the edge beam are due to the axial load in the beam as well as to couples that exist about the beams' major and minor axes.

With this as a guide we state the condition of junction strain compatibility between beam and slab as follows.

$$E^{-1}\sigma_r - E^{-1}(\sigma_{xx} - \mu\sigma_{yy}) = 0 \tag{24}$$

where σ_r, the beam stress, is given by

$$\sigma_r = -(P - F)/A_r + E\bar{h}w_{,xx} - \frac{Eb_r}{2}u_{y,xx}. \tag{25}$$

A_r is the beam cross-sectional area.

Substituting for F, w, u_y, σ_{xx}, σ_{yy}, eqns (24) and (25) combine to yield the relations

$$[\lambda_m \bar{h} ch\psi_m]A_{m1} + [\lambda_m \bar{h}\psi_m sh\psi_m]D_{m1} + E^{-1}\left[sh\psi_m \cdot \frac{t}{A_r} + (1-\mu)\lambda_m ch\psi_m + (1+\mu)\frac{\lambda_m^2 b_r}{2} sh\psi_m\right]A_{m2}$$
$$+ E^{-1}\left[(\psi_m ch\psi_m + sh\psi_m)\frac{t}{A_r} + \lambda_m(1+\mu)\psi_m sh\psi_m + 2ch\psi_m)\right.$$
$$\left. + \frac{\lambda_m^2 b_r}{2}((1+\mu)\psi_m ch\psi_m - (1-\mu)sh\psi_m)\right]D_{m2}$$
$$+ E^{-1}\sum_{s=1}^{\infty}\sum_{r=1}^{\infty} L_{mr}[G_{rs}A_{s2} + F_{rs}D_{s2}] = -\frac{4(EA)^{-1}P}{\lambda_m^2 a} \tag{26}$$

where

$$L_{mr} = \frac{8}{a^2} \cdot \frac{\alpha_r(\alpha_r^2 - \mu\lambda_m^2)(1 + ch\alpha_r a)}{(\lambda_m^2 + \alpha_r^2)}. \tag{27}$$

To arrive at eqns (26) and (27) we employ the mathematical technique of taking out certain superposition coefficients from under the summation signs relying on the well known trigonometric orthogonality relations and the definite integral

$$\int_0^a \left[\alpha_r(x-a)sh\alpha_r x + \alpha_r x sh\alpha_r(x-a) + \frac{2\mu}{1+\mu}\{ch\alpha_r x + ch\alpha_r(x-a)\}\right]\sin\lambda_m x\, dx$$
$$= \frac{4(\alpha_r^2 - \mu\lambda_m^2)(1 + ch\alpha_r a)}{(\lambda_m^2 + \alpha_r^2)^2}. \tag{28}$$

Equilibrium about the minor axis

Considering the horizontal equilibrium of the beam of Fig. 2 and the bending moment about its minor axis we have

$$\delta N - (t\sigma_{yyb})\delta x = 0 \tag{29}$$

$$\delta_m = N \cdot \delta x - \frac{b_r}{2}\delta F. \tag{30}$$

Equations (29) and (30) combine to give

$$m_{,xx} - t\sigma_{yyb} + \frac{b_r}{2} \cdot F_{,xx} = 0. \tag{31}$$

Taking $m = -Eiu_{y,xx}$ and noting that $F_{,xx} = -t\phi_{,xxy|y=b}$, eqn (31) now takes the form

$$-Eiu_{y,xxxx} - t\sigma_{yyb} - \frac{tb_r}{2}\phi_{,xxy|y=b} = 0. \tag{32}$$

Substituting for u_y, σ_{yy}, & $\phi_{,xxy|y=b}$ and performing the now familiar mathematical techniques previously employed we arrive at

$$\left[(1+\mu)\lambda_m^3 ish\psi_m + tch\psi_m + \frac{\lambda_m b_r}{2} \cdot tsh\psi_m\right]A_{m2}$$
$$+ \left[(1+\mu)\lambda_m^3 i\left(\psi_m ch\psi_m - \frac{1-\mu}{1+\mu}sh\psi_m\right) + t\psi_m sh\psi_m + \frac{\lambda_m b_r}{2}t(\psi_m ch\psi_m + sh\psi_m)\right]D_{m2}$$
$$- t\sum_{s=1}^{\infty}\sum_{r=1}^{\infty} H_{mr}[G_{rs}A_{s2} + F_{rs}D_{s2}] = 0 \tag{33}$$

where H_{mr} is as previously defined in (21).

Loading

The loading to be applied here is the combination of the prestressing force and lateral loading on the edge beams. The prestressing force is assumed to have a parabolically varying eccentricity relative to the centroid of the edge beam cross-section and having a maximum value at midspan. We also present expressions that will enable us solve for cases of superimposed loading on the beams and slab.

By adopting a Fourier series representation for the loading, the Fourier coefficient of each harmonic component of the loading is

$$P_n = -\frac{32Pe_m}{\lambda_n a^3} - \frac{EIq_n}{D} + \frac{4p}{\lambda_n a} + \frac{2W}{a} \cdot \sin\left(\frac{n\pi}{2}\right)$$

where q_n is the slab superimposed loading, P the prestressing force of maximum eccentricity e_m, p the uniformly distributed loading and W the midspan point loading on the edge beam.

NUMERICAL EXAMPLES

Two cross-sections, shown in Fig. 3, are adopted as the edge beams for purposes of computations. Further particulars of the adopted sections are given in Table 1 below.

Table 1

Property	Rectangular Section	Inverted T-Section
Breadth	0.491 m	0.225 m
Depth	1.05 m	1.20 m
Area	0.5156 m^2	0.36 m^2
Second Moment of Area, I	0.047 366 m^4	0.047 324 m^4
Second Moment of Area, i	0.010 375 m^4	0.004 331 m^4
Polar Second Moment of Area, J	0.028 462 m^4	0.006 341 m^4
Eccentricity of Prestressing Force	0.175 m	0.1846 m

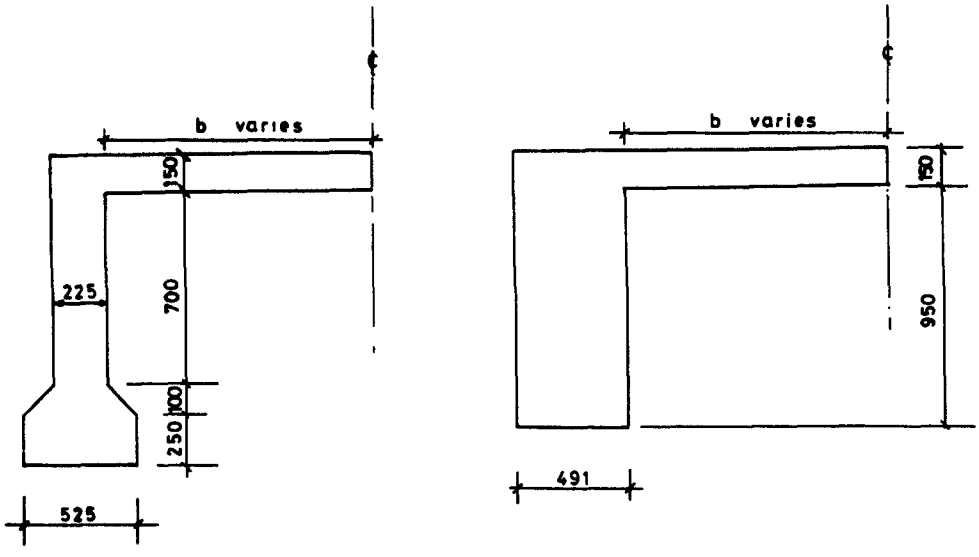

Dimensions in millimetres

Fig. 3.

Other data relevant to the analysis are: slab thickness 0.15 m; span 10.0 m; modulus of elasticity 21×10^6 kN/m^2; Poisson's ratio 0.15. In addition, the effect of changes in edge beam properties like flexural rigidities about the major and minor axes, torsional rigidity and cross-sectional area, is investigated by adopting an edge beam of rectangular section and varying the depth. Results relating to these changes of edge beam properties are better presented in terms of edge beam depth to slab thickness ratio, H/t. An average direct stress of 14,000 kN/m^2 is assumed as the initial prestress of the rib alone, while we adopt a transverse point load of 1100 kN and uniformly distributed load of 220 kN/m, applied on the edge beams.

Computations

Equations (17), (20), (26) and (33) are the set of linear equations that are solved to determine the four superposition coefficients A_{r1}, D_{r1}, A_{r2} and D_{r2} appearing in those equations. We note that eqn (33) contains only the superposition coefficients A_{r2} and D_{r2} of the stress function ϕ, while eqns (17), (20) and (26) contain the superposition coefficients A_{r1} and D_{r1} of the deflexion field in addition to A_{r2} and D_{r2}. By eliminating the superposition coefficients A_{r1} and D_{r1} from these last three equations, we reduce them to one equation involving only A_{r2} and D_{r2}, so that we are now left with two equations involving A_{r2} and D_{r2} to program for the computer. Once we solve for these sets of superposition coefficients, we obtain the A_{r1}'s and D_{r1}'s by back substitution.

Once we have obtained these superposition coefficients, the deflexion field and the stress field are quantitatively defined. In beam–slab interaction, in addition to pure bending of the two interacting elements, both elements develop equal but opposite interacting axial forces that alter their stress distributions from the pure bending distributions and hence alter their deflexion profiles. It is therefore convenient, in the present case, to define the effective width of a slab as that portion of its width having across it a constant stress, equal in magnitude to the stress in the slab at its junction with the edge beam and thereby sustaining a force equal in magnitude to the interacting axial force in each of the elements.

We may further define effective width factor as the fractional ratio of the effective width of a slab interacting with an edge beam to its actual width available for developing the interacting axial force in the slab. We express this mathematically as follows:

$$\beta = \frac{F}{bt\sigma_{xx|y=b}} = \frac{-\phi_{,y|y=b}}{b\phi_{,yy|y=b}}. \tag{34}$$

It is obvious that eqn (34) will only involve the superposition coefficients A_{r2} and D_{r2}.

The computer program is developed, not only to solve for the superposition coefficients appearing in eqns (17), (20), (26) and (33), but also to compute deflexions, stresses in edge beams and the slab, the interacting axial forces and the effective width factors. The results are given in Tables 2–4 in Figs. 3–7.

DISCUSSION OF RESULTS

Figures 4–6 and 4(a), 5(a) and 6(a) depict the characteristics under load of the edge beams when they are of inverted T section and rectangular section respectively.

(i) *Redistribution of prestress*

Figures 4 and 4(a) show that there is a transfer of the prestress from the beams to the slab. We also observe that under prestress alone, only a small fraction of the prestressing force is transferred to the slab; this is due to the effect of bending of the section caused by eccentricity of the prestressing force. We note however, that under live load, when the bending effect is opposite to the prestressing one, the compressive force in the slab becomes appreciable.

Table 2. Effective width factors for prestressed L-beams under different loading conditions

b/a	I-section Rib			Rectangular Section Rib		
	Prestress alone	Prestress+ Point Load	Prestress+ u.d.l	Prestress alone	Prestress + Point Load	Prestress + u.d.l
0	1.0	1.0	1.0	1.0	1.0	1.0
0.1	-	-	0.926	-	-	0.922
0.2	0.730	0.669	0.817	0.814	0.688	0.822
0.3	0.754	0.509	0.654	0.788	0.528	0.656
0.4	0.627	0.386	0.500	0.633	0.400	0.400
0.5	0.480	0.301	0.388	0.482	0.311	0.387
0.6	0.369	0.244	0.311	0.372	0.251	0.310
0.7	0.293	0.204	0.258	0.296	0.209	0.255
0.8	0.239	0.174	0.218	0.243	0.178	0.216
0.9	0.201	0.152	0.189	0.205	0.155	0.186
1.0	0.173	0.135	0.166	0.177	0.136	0.164

Table 3. Effective width factors for non-prestressed L-beams, under different loading conditions

b/a	I-Section Rib		Rectangular Rib	
	Points Load	u.d.l	Point Load	u.d.l
0	1.0	1.0	1.0	1.0
0.1	-	0.951	-	0.953
0.2	0.665	0.825	0.671	0.823
0.3	0.494	0.646	0.500	0.640
0.4	0.372	0.491	0.376	0.485
0.5	0.290	0.381	0.291	0.375
0.6	0.235	0.307	0.236	0.301
0.7	0.197	0.255	0.197	0.249
0.8	0.169	0.217	0.169	0.212
0.9	0.148	0.188	0.148	0.183
1.0	0.131	0.166	0.130	0.162

Table 4. Variation of effective width factors wit bending and torsional rigidities

H/t \ b/a	0.0	0.2	0.4	0.6	0.8	1.0
2.0	1.0	0.656	0.360	0.222	0.158	0.122
4.0	1.0	0.667	0.378	0.237	0.169	0.130
6.0	1.0	0.680	0.392	0.246	0.175	0.134
8.0	1.0	0.696	0.409	0.256	0.181	0.139
10.0	1.0	0.715	0.428	0.267	0.188	0.143
12.0	1.0	0.735	0.449	0.279	0.195	0.149
14.0	1.0	0.758	0.471	0.292	0.203	0.154
16.0	1.0	0.781	0.495	0.306	0.212	0.160
18.0	1.0	0.807	0.519	0.320	0.220	0.165
20.0	1.0	0.832	0.544	0.334	0.229	0.171

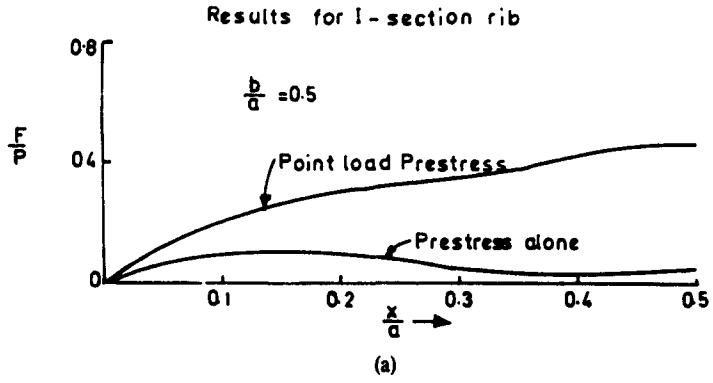

(a)

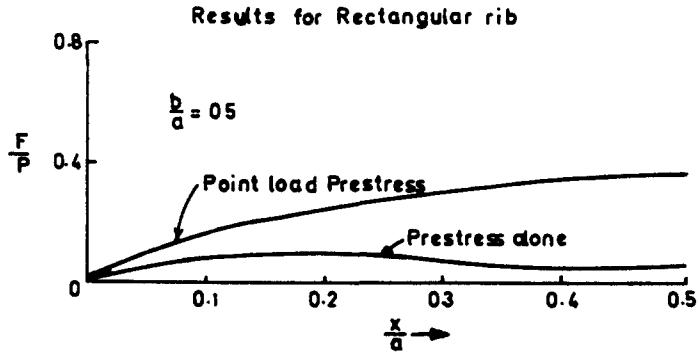

(b)

Fig. 4.

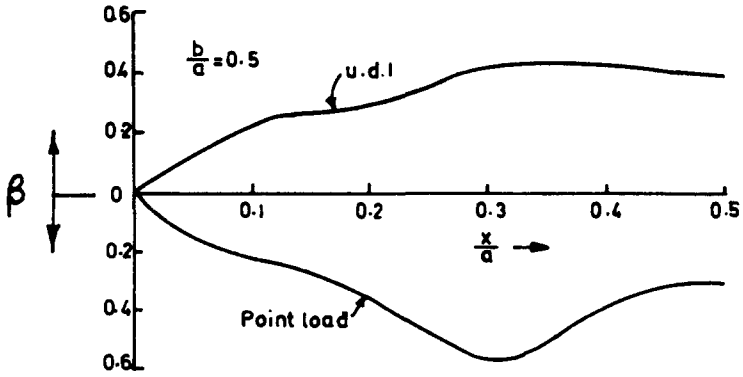

(a)

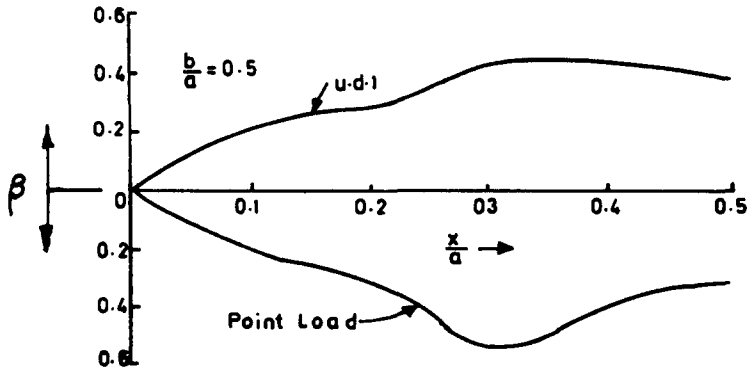

(b)

Fig. 5.

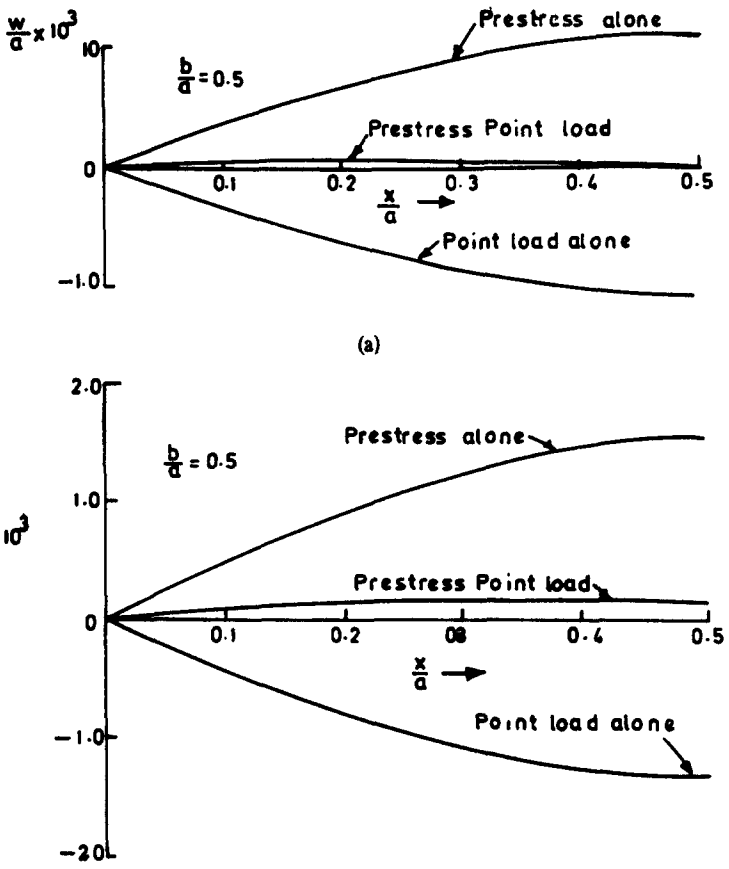

Fig. 6.

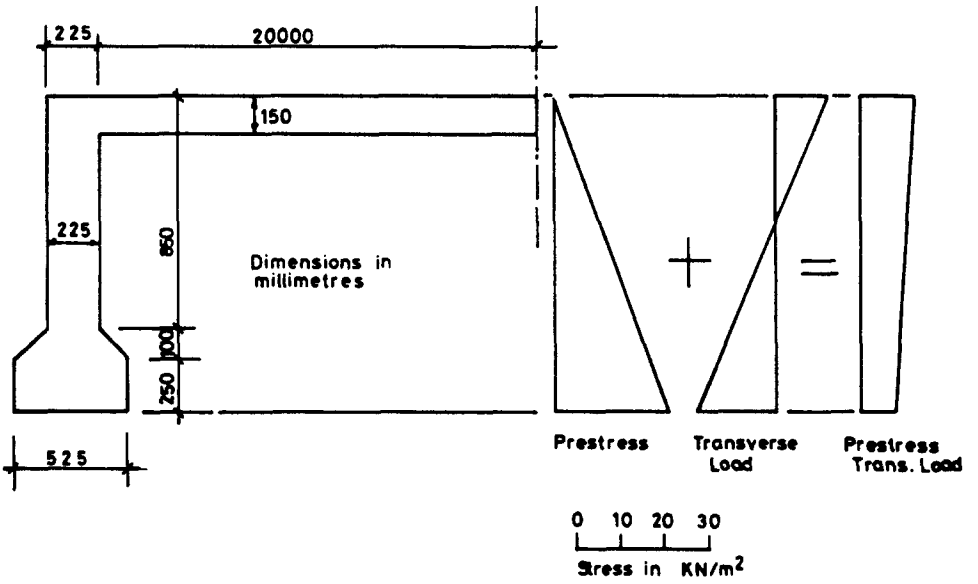

Fig. 7.

(ii) *Variation of effective widths*

Figures 5 and 5(a) show the variation of effective width factor, β, along the span for both uniform loading and point loading for the two cross-sections considered. The curves for each type of loading for the two cross-sections show similar trend, with the values of effective width factors applicable to the rectangular edge beam being slightly higher than those applicable to

the inverted T-beam for the point loading case, while values for the uniform loading are of the same order of magnitude for both types of beams. Tabulated figures in Table 2 gives the relative magnitudes of effective width factors of slab applicable to the two types of edge beams adopted for different beam loading.

An examination of these figures confirms the preceding observations in respect of effective width factor variation for the edge beams considered under both point load and uniform loading. The Table also presents effective width factors due to the effect of prestressing alone. At low aspect ratios of the slab, there are differences between the values for the two types of edge beams in respect of prestressing alone, whereas at aspect ratios of between 0.4 and 1.0 these differences become insignificant.

Tabulated values of slab effective width factors for the non-prestressed, non-reinforced sections, assumed "elastic", are presented in Table 3 for point load and uniform loading. It is significant that values obtained for the non-prestressed, non-reinforced edge beam case (always assuming that the materials are elastic and can resist tension) and those obtained when the edge beams are prestressed are of the same order of magnitude for the same type of transverse loading. This is most probably due to the fact that the flexural and torsional rigidities of each type of edge beam considered will remain nearly constant in both cases. Steel reinforcement in the beams which would materially alter these rigidities could have produced significantly different values of effective width factors for the same beam cross-section. Since flexural and torsional rigidities depend partly on the geometry of the cross-section, these properties are difficult to vary individually in a physically realisable cross-section. In order to study the effect of changes in these properties of a section therefore, we adopt a rectangular cross-section of fixed width but variable depth. We achieve this by varying the beam depth to slab thickness ratio as a measure of the changes in these properties in a manner consistent with the assumed rectangular geometry. Table 4 presents the variation of effective width factors with slab aspect ratio and H/t ratios. It is obvious from these results that effective widths of slabs are dependent on the flexural and torsional rigidities of the edge beams with which they interact—in addition to their dependence on aspect ratios of the slabs themselves. The slab is made to participate more fully as flexural and torsional rigidities of the edge beams increase.

(iii) *Transverse deflexion*

Figures 6 and 6(a) present the transverse deflexion behaviour of the two types of edge beams under the loadings indicated. Apart from demonstrating the response of the sections to prestressing and transverse loading, the figures show that the inverted T-rib exhibits higher overall flexural resistance, in its deflection values, on interaction with the slab. This may be because when the width of slab interacting with a beam is known, the resulting composite section for the inverted T-rib yields higher flexural rigidities than the corresponding ones for a rectangular rib.

(iv) *Computation of stresses*

Finally we present in Fig. 7 the stress blocks in one of the two types of edge beams adopted due to "prestressing", "tranverse loading" and "prestress plus transverse loading". These results demonstrate that the equations derived in the present analysis may find ready application in the evaluation of alternative sections for this type of bridge-deck system especially if the interest is on assessment of deflexions and the stresses induced under different transversely symmetric loading conditions. Once the program is developed, results of alternative designs by the adoption of different cross-sections can be quickly assessed.

CONCLUSIONS

The analysis shows that effective width applicable to a rectangular slab stiffened by two identical prestressed edge beams is not different from that for the case with unreinforced stiffening edge beams. The prestressing force needed for resisting live load, can sufficiently be estimated on the basis of the edge beam cross-sectional area alone carrying all the prestress. In other words there is no need to consider any portion of the slab as acting with the beam in estimating the required prestressing load.

If the prestressing of the edge beams is done after the beam and slab had been cast, then average compressive stress in the edge beam could be taken 0.6 of the maximum permissible concrete compressive stress, since part of the prestressing load will be transferred to the concrete slab deck. Where the edge beam cross-section is not simply rectangular, an equivalent rectangular section having the same flexural rigidity, assuming a breadth equal to the web breadth, could be determined for the purpose of estimating H/t in order to find the applicable effective width factor.

REFERENCES

1. D. N. deG. Allen and R. T. Severn, Composite action of beams and slabs under transverse loading. *Struct. Engng* **39**(7), 235–239 (1961).
2. A. O. Adekola, Effective width of composite beams of steel and concrete, *Struct. Engng* **46**(9), 285–289 (1965).
3. A. O. Adekola, The dependence of shear lag on partial interaction in composite beams. *Int. J. Solids Structures* **10**, 389–400 (1974).